



**HAL**  
open science

## Temperature seasonality regulates organic carbon burial in lake

Shengfang Zhou, Hao Long, Weizhe Chen, Chunjing Qiu, Can Zhang, Hang Xing, Jingran Zhang, Liangqing Cheng, Cheng Zhao, Jun Cheng, et al.

► **To cite this version:**

Shengfang Zhou, Hao Long, Weizhe Chen, Chunjing Qiu, Can Zhang, et al.. Temperature seasonality regulates organic carbon burial in lake. *Nature Communications*, 2025, 16 (1), pp.1049. 10.1038/s41467-025-56399-4 . hal-04940378

**HAL Id: hal-04940378**

**<https://hal.science/hal-04940378v1>**

Submitted on 11 Feb 2025

**HAL** is a multi-disciplinary open access archive for the deposit and dissemination of scientific research documents, whether they are published or not. The documents may come from teaching and research institutions in France or abroad, or from public or private research centers.

L'archive ouverte pluridisciplinaire **HAL**, est destinée au dépôt et à la diffusion de documents scientifiques de niveau recherche, publiés ou non, émanant des établissements d'enseignement et de recherche français ou étrangers, des laboratoires publics ou privés.


# Temperature seasonality regulates organic carbon burial in lake

Received: 9 November 2024

Accepted: 17 January 2025

Published online: 26 January 2025


 Check for updates

Shengfang Zhou<sup>1,2,3,13</sup>, Hao Long<sup>1,2,4,13</sup> , Weizhe Chen<sup>5,13</sup>, Chunjing Qiu<sup>6</sup>, Can Zhang<sup>1,2</sup>, Hang Xing<sup>7</sup>, Jingran Zhang<sup>8,9</sup>, Liangqing Cheng<sup>1,2</sup>, Cheng Zhao<sup>10</sup>, Jun Cheng<sup>11</sup>  & Philippe Ciais<sup>12</sup>

Organic carbon burial (OCB) in lakes, a critical component of the global carbon cycle, surpasses that in oceans, yet its response to global warming and associated feedbacks remains poorly understood. Using a well-dated biomarker sequence from the southern Tibetan Plateau and a comprehensive analysis of Holocene total organic carbon variations in lakes across the region, here we demonstrate that lake OCB significantly declined throughout the Holocene, closely linked to changes in temperature seasonality. Process-based land surface model simulations clarified the key impact of temperature seasonality on OCB in lakes: increased seasonality in the early Holocene saw warmer summers enhancing ecosystem productivity and organic matter deposition, while cooler winters improved organic matter preservation. The Tibetan Plateau's heightened sensitivity to climate and ecosystem dynamics amplifies these effects. With declining temperature seasonality, we predict a significant slowdown or reduction in OCB across these lake sediments, leading to carbon emissions and amplified global warming.

Lakes cover only 1.8% of the Earth's surface<sup>1</sup>, yet the sequestration of organic carbon (OC) in lake sediments is comparable to, or even exceeds, that in marine sediments and soils<sup>2–4</sup>. Temperature exerts a critical influence on the sequestration of OC within lake sediments<sup>5–8</sup>. On one hand, warming enhances ecosystem productivity, leading to increased OC input into sediments for sequestration; on the other hand, it accelerates decomposition, resulting in higher mineralization and reduced burial efficiency<sup>6,9,10</sup>. Consequently, the response of

net OC sequestration to global warming remains uncertain. A recent study examining OC accumulation during the Medieval Warm Period and the Recent Warming Period<sup>11</sup> highlights the contrasting responses of OC accumulation to warming during the growing and the non-growing seasons (as demonstrated in Fig. 1a, b). This underscores the need to elucidate how seasonal temperature variations influence organic carbon burial (OCB) to better predict future dynamics in carbon cycles.

<sup>1</sup>Key Laboratory of Lake and Watershed Science for Water Security, Nanjing Institute of Geography and Limnology, Chinese Academy of Sciences, Nanjing, China. <sup>2</sup>State Key Laboratory of Lake Science and Environment, Nanjing Institute of Geography and Limnology, Chinese Academy of Sciences, Nanjing, China. <sup>3</sup>University of Chinese Academy of Sciences, Beijing, China. <sup>4</sup>University of Chinese Academy of Sciences, Nanjing, China. <sup>5</sup>State Key Laboratory of Biogeology and Environmental Geology, Hubei Key Laboratory of Critical Zone Evolution, School of Earth Sciences, China University of Geosciences, Wuhan, China. <sup>6</sup>Research Center for Global Change and Ecological Forecasting, School of Ecological and Environmental Sciences, East China Normal University, Shanghai, China. <sup>7</sup>Key Laboratory of Humid Subtropical Eco-geographical Process (Ministry of Education), School of Geographical Sciences, Fujian Normal University, Fuzhou, China. <sup>8</sup>School of Geography, Nanjing Normal University, Jiangsu Centre for Collaborative Innovation in Geographical Information Resource Development and Application, Nanjing, China. <sup>9</sup>Key Laboratory of Virtual Geographic Environment, Ministry of Education, Nanjing, China. <sup>10</sup>School of Geography and Ocean Science, Nanjing University, Nanjing, China. <sup>11</sup>School of Marine Sciences, Nanjing University of Information Science and Technology, Nanjing, China. <sup>12</sup>Laboratoire des Sciences du Climat et de l'Environnement, LSCE/IPSL, CEA-CNRS-UVSQ, Université Paris-Saclay, Gif-sur-Yvette, France. <sup>13</sup>These authors contributed equally: Shengfang Zhou, Hao Long, Weizhe Chen.  e-mail: [longhao@niglas.ac.cn](mailto:longhao@niglas.ac.cn); [chengjun@nuist.edu.cn](mailto:chengjun@nuist.edu.cn)

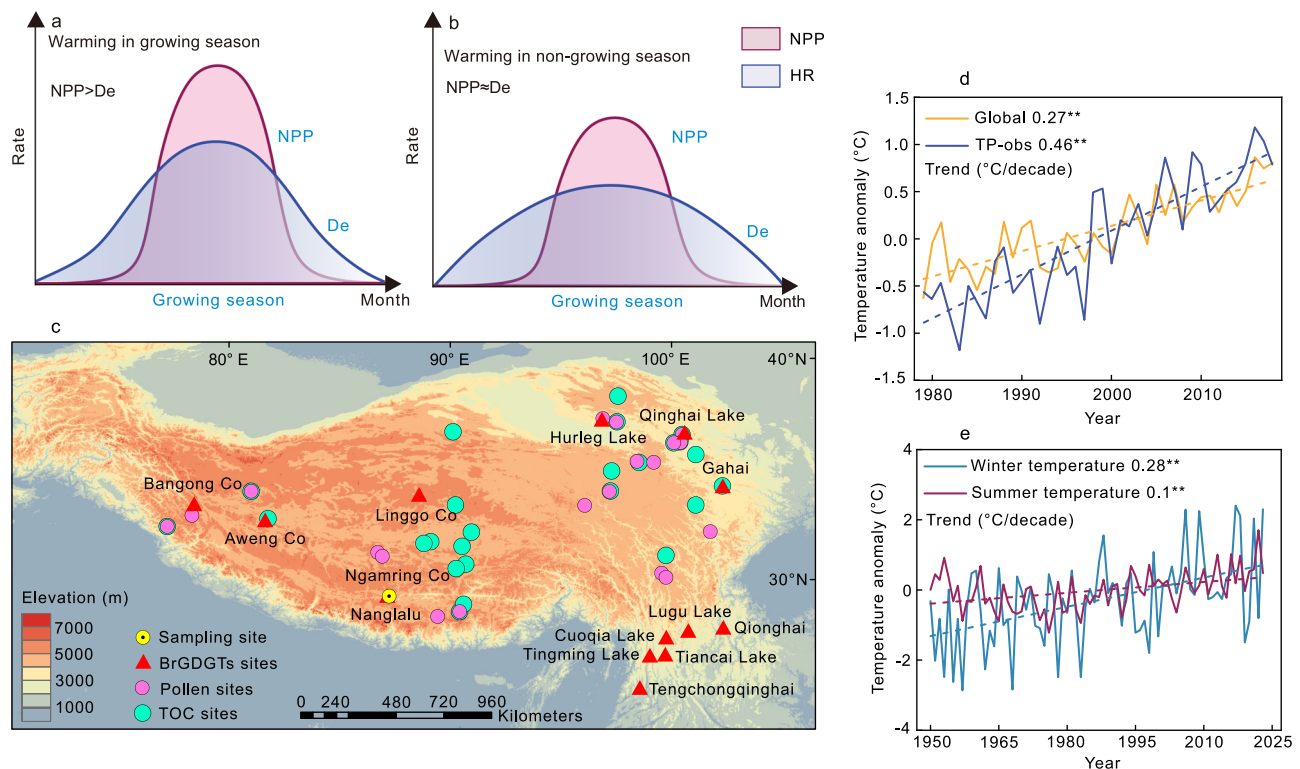


**Fig. 1 | Impacts of seasonal warming on carbon dynamics and study area.** Net carbon balance in lake sediments in response to warming during **a** growing season and **b** non-growing season (NPP: net primary productivity, De: decomposition). Warming during the growing season results in  $NPP > De$ , leading to increased carbon accumulation, while warming during the non-growing season enhances De, potentially offsetting NPP, leading to less accumulation of carbon loss. **c** Study area and published records of branched glycerol dialkyl glycerol tetraethers (brGDGTs),

pollen, and TOC on the Tibetan Plateau (Supplementary Tables 1, 2, 3). **d** Time series and trends of annual surface mean temperature anomalies during 1979–2018 over the Tibetan Plateau (TP-obs)<sup>14</sup> and the global mean<sup>15</sup>. The trends that passed the significance test ( $p < 0.05$ ) in the two-tailed test are marked with double asterisks. **e** Summer and winter surface mean temperature anomalies (1950–2022) for the Tibetan Plateau, derived from ERA data<sup>15</sup>. The trends that passed the significance test ( $p < 0.05$ ) in the two-tailed test are marked with double asterisks.

The Tibetan Plateau, often referred to as the Third Pole<sup>12,13</sup> (Fig. 1c), is warming at an accelerated rate of approximately 0.46 °C per decade<sup>14</sup>, nearly twice the global average of approximately 0.27 °C per decade<sup>15</sup> (Fig. 1d). During the period from 1950 to 2022, winter temperatures on the plateau increase significantly faster than summer temperatures (Fig. 1e). Additionally, the Tibetan Plateau hosts 1424 lakes larger than 1 km<sup>2</sup>, collectively covering an area of 50,323 km<sup>2</sup> as of 2018<sup>16</sup>, making lakes a crucial component of the regional carbon cycle<sup>17,18</sup>. Between 1984 and 2023, lakes on the Tibetan Plateau stored approximately 32.8 Tg C of dissolved organic carbon (DOC), accounting for about 83.2% of total DOC in Chinese lakes<sup>19</sup>. Notably, 92% of the increase in DOC storage occurred on the Tibetan Plateau<sup>19</sup>. Nevertheless, CO<sub>2</sub> emissions from these lakes have been continuously increasing<sup>20</sup>. These unique characteristics position the Tibetan Plateau as a natural laboratory for exploring the relationship between seasonal temperature variations and changes in carbon content in lake sediment. Despite its significance, research integrating long-term quantitative temperature reconstructions with OCB records on the Tibetan Plateau is scarce. Furthermore, the absence of mechanistic interpretations combining terrestrial carbon cycle models with paleoclimate models hinders a comprehensive understanding on the response of OCB in lake sediments to seasonal temperature variations in polar and alpine environments.

In this study, we present records of branched glycerol dialkyl glycerol tetraethers (brGDGTs) and n-alkanes derived from a well-dated lacustrine sediment sequence in Lake Nanglalu, southern Tibet (Fig. 1c, Supplementary Fig. 1, Supplementary Discussion for a characterization of regional setting and sampling, Supplementary Data 1), to quantify Holocene variations in temperature and OCB. Our

reconstructed temperature record is compared with published lake brGDGT sequences and seasonal temperature simulations from the transient climate simulation of the Last 21,000 Years (TraCE-21ka)<sup>21,22</sup>. Additionally, we expand our dataset to include 45 published total organic carbon (TOC) and pollen concentration records across the Tibetan Plateau to investigate how OCB responds to seasonal temperature variations. Finally, a process-based ORCHIDEE (Organizing Carbon and Hydrology in Dynamic Ecosystems) model<sup>23</sup> was employed to simulate the terrestrial organic carbon cycling processes and uncover the mechanisms behind OCB's response to temperature seasonality during the Holocene. Our results, in conjunction with the synthesis of the published TOC dataset, suggest an increased OCB during periods of heightened temperature seasonality on the Tibetan Plateau in the early-to-middle Holocene relative to the middle-to-late Holocene. This indicates a positive relationship between regional temperature seasonality and OCB in lakes. These findings can help in predicting long-term OCB dynamics in the context of global warming characterized with weakening temperature seasonality (Fig. 1e).

## Results and discussion

### Seasonal biases in brGDGTs-based temperatures on the Tibetan Plateau

BrGDGTs have two C<sub>28</sub> alkyl chains with 4–6 methyl substituents and 0–2 cyclopentyl moieties, which have been extensively used as paleothermometers. This is due to the ability of the producers of these compounds to alter the fluidity of their lipid membranes in response to temperature variations<sup>24–29</sup>. In the Nanglalu record, the brGDGT-based temperatures reveal a distinct two-phase pattern throughout the

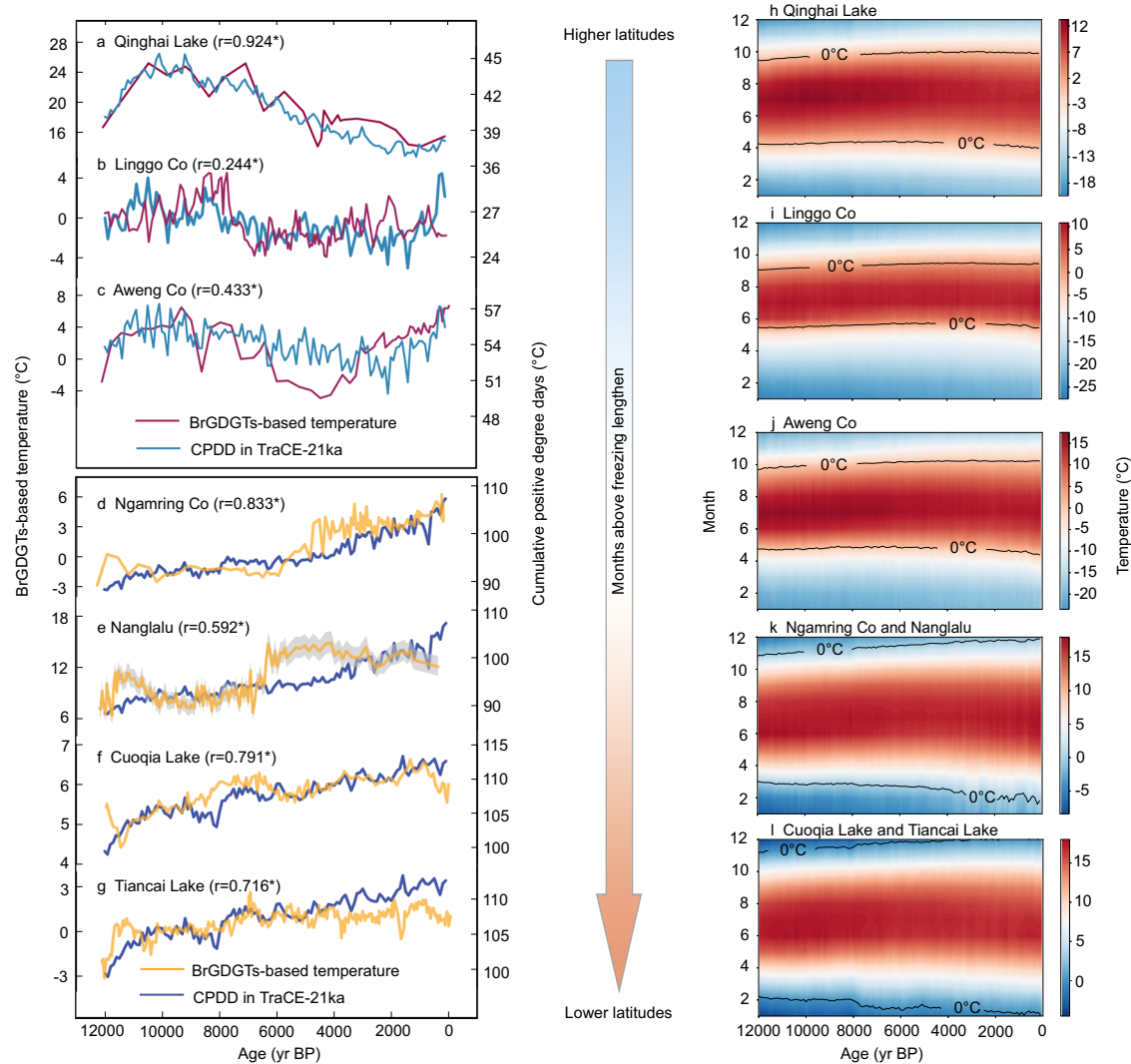


**Fig. 2 | Comparison of temperature reconstruction and simulation for different lake sites. a** Qinghai Lake<sup>31</sup>. **b** Linggo Co<sup>32</sup>. **c** Aweng Co<sup>33</sup>. **d** Ngamring Co<sup>34</sup>. **e** Nanglalu (in this study, the yellow solid line represents the temperature calculated using calibration formula reported by Martínez-Sosa<sup>27</sup>, with the shaded area indicating the 95% confidence interval). **f** Cuoqia Lake<sup>35</sup>. **g** Tiancai Lake<sup>36</sup>. Pearson

correlation analysis was performed between brGDGTs-based temperatures and cumulative positive degree days (CPDD) data extracted from Liu<sup>22</sup>. Asterisks indicate that the correlation is statistically significant at the 0.01 level based on a two-tailed test. **h–l** Isothermal maps of monthly temperatures during the Holocene in TraCE-21ka<sup>22</sup>.

Holocene: a cooler period from the Early-to-Mid Holocene (EMH, -12 to 6.5 ka BP), followed by a warming trend from the mid-Holocene to the present (-6.5 to present) (Supplementary Figs. 2 and 3, Supplementary Discussion for a characterization of BrGDGTs-based temperature reconstruction in the Nanglalu). The methylation positions of brGDGTs in Nanglalu differ significantly from those in surface soils on the Tibetan Plateau<sup>30</sup> (Supplementary Fig. 4). Additionally, based on the carbon number distribution of n-alkanes from Nanglalu (Supplementary Fig. 5), it can be inferred that Nanglalu predominantly represented a shallow lake or wetland depositional environment during the Holocene, with minimal terrestrial input from the surrounding watershed. Based on these observations, we conclude that the brGDGTs in Nanglalu are primarily of lacustrine origin. Therefore, the temperature reconstructed from brGDGTs mainly reflects lake water temperature. We combined brGDGTs record of Nanglalu with 13 published lake sediment brGDGT records across the Tibetan Plateau<sup>31–36</sup> (Fig. 1c, Supplementary Table 1). The majority of these lake sediment brGDGTs are of lacustrine origin (Supplementary Table 1). We further observed that temperature variation patterns of these lakes are latitude-dependent. Specifically, in higher-altitude regions, brGDGTs-based temperatures in lake sediments

generally increased during the EMH, reaching their maximum before subsequently decreasing and then steadily rising again from the middle Holocene onward (Fig. 2a–c, Supplementary Fig. 6A). In contrast, in lakes from lower-latitude regions, brGDGTs-based temperatures show a continuous warming trend throughout the Holocene (Fig. 2d–g, Supplementary Fig. 6B). We further compared these brGDGT records with TraCE-21ka simulated annual mean temperatures and seasonal temperatures. It was found that lakes at higher latitudes exhibit contrasting trends between brGDGT-based temperatures and both modeling annual and winter mean temperatures (Supplementary Figs. 7A and 8A), but show greater alignment with summer mean temperatures (Supplementary Fig. 9A). In contrast, lower-latitude lakes demonstrate opposing trends between brGDGT-based temperatures and summer mean temperatures (Supplementary Fig. 9B), while annual and winter mean temperatures reveal closer consistency (Supplementary Fig. 7B, 8B). Notably, nearly all brGDGTs-based temperature records from lakes on the Tibetan Plateau correlate well with the cumulative positive degree days data extracted from TraCE-21ka (Fig. 2a–g, Supplementary Figs. 10 and 11). According to the TraCE-21ka modeling data, we observed similar meridional changes in the duration of above-freezing

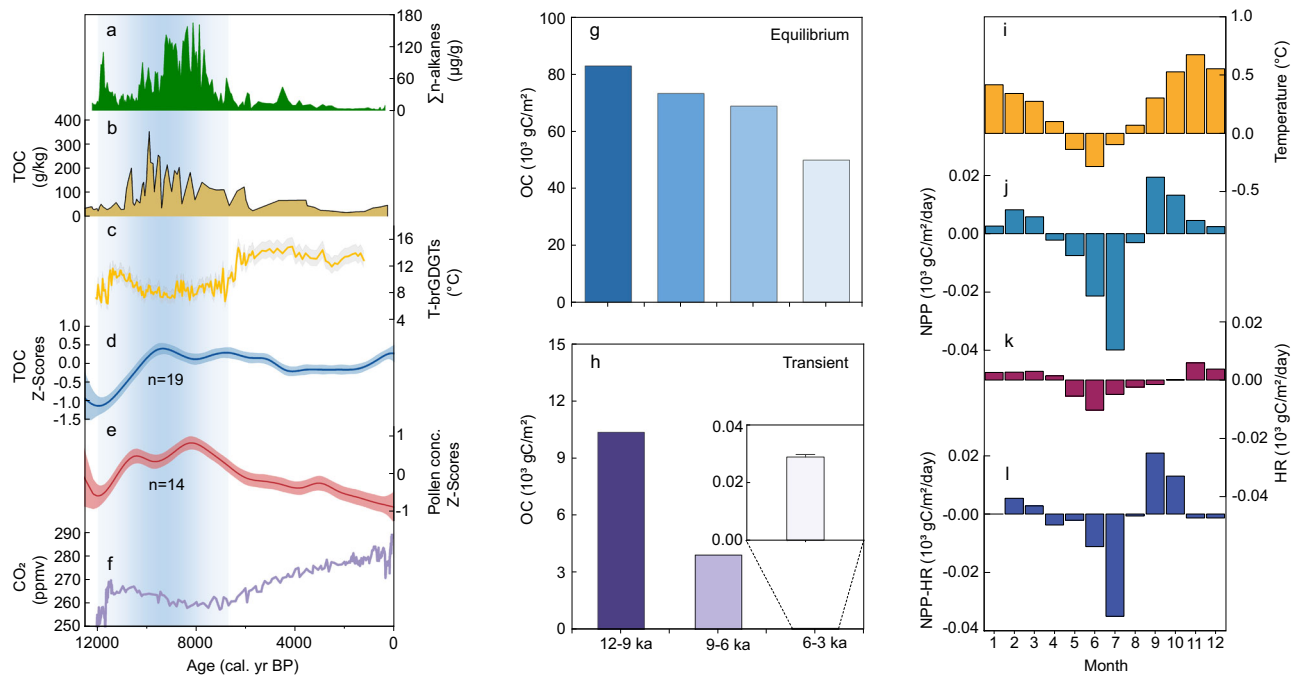


**Fig. 3 | Impacts of temperature on organic carbon burial.** **a** Total n-alkane content in the Nanglalu. **b** Total organic carbon (TOC) in Nanglalu<sup>44</sup>. **c** BrGDGTs-based temperature reconstruction for Nanglalu, with the shaded area representing the 95% confidence interval. **d** Integrated analysis of TOC across the Tibetan Plateau, with the blue curve representing the Generalized Additive Model (GAM) fit and the shaded area indicating the 95% confidence interval. **e** Integrated analysis of pollen concentration across the Tibetan Plateau, with the red curve representing

the GAM fit and the shaded area indicating the 95% confidence interval. **f** Global CO<sub>2</sub> reconstruction<sup>39</sup>. In **a–f**, the blue gradient bar highlights the Early to Mid-Holocene period. **g, h** Equilibrium and transient simulations of organic carbon stock, respectively, based on the ORCHIDEE model in this study. **i–l** Linear trends from the early to late Holocene for temperature (**i**), net primary productivity (NPP) (**j**), heterotrophic respiration (HR) (**k**) and NPP-HR (**l**). Results for NPP, HR and NPP-HR are from transient simulation.

temperatures throughout the year, which expanded as latitude decreased (Fig. 2h–l).

The presence of ice cover may inhibit the activity of brGDGT producers<sup>37</sup>, and the ice layer restricts thermal exchange between lake water and the atmosphere<sup>38</sup>. As a result, temperatures recorded by brGDGTs tend to reflect only the months above freezing<sup>27,28,35</sup>. Notably, in lower-latitude regions, the temperature reconstructed from brGDGTs during months above freezing shows a persistent increasing trend throughout the Holocene, while summer temperatures simulated at the same grid points exhibit a long-term decreasing trend (Supplementary Fig. 9B). For the Tibetan Plateau, the overall decline in summer temperatures during the Holocene is also supported by temperature reconstructions based on alkenones and chironomids (Supplementary Fig. 12A, B). This phenomenon highlights a contradiction between the rising trend in months above freezing temperatures and the declining trend in summer temperatures. In lower-latitude regions, the months above freezing encompass not only the summer season but also parts of spring, autumn, and even winter (Fig. 2k, l). These periods are collectively referred to as non-summer months. Simulations from TraCE-21ka indicate that the temperatures during these non-summer months have consistently increased throughout the Holocene (Supplementary Fig. 13). The rising trend in non-summer temperatures likely compensates for the declining summer temperatures, resulting in an overall increase in months above freezing temperatures at lower latitudes (Fig. 2d–g, Supplementary Fig. 10B). In contrast, at higher latitudes, the shorter duration of months above freezing minimizes the contribution of non-summer temperatures to the cumulative thermal energy (Fig. 2h–j). As such, the variability in months above freezing temperatures more resembles that of summer temperatures. However, since the Mid- to Late Holocene, increasing atmospheric CO<sub>2</sub> concentrations<sup>39</sup> may have led to an extension of the months above freezing, causing months above

freezing temperatures at higher latitudes to decouple from summer temperatures and exhibit a persistent upward trend (Supplementary Fig. 9A).

Consequently, on the Tibetan Plateau, temperatures reconstructed from brGDGTs reflect the temperature above freezing, which align well with the cumulative positive degree days simulations from TraCE-21ka (Fig. 2a–g, Supplementary Fig. 10, 11). We thus introduce the cumulative positive degree days (CPDD) to interpret the brGDGTs-based temperature reconstructions on the Tibetan Plateau. CPDD is particularly useful for two reasons: first, it better captures changes in the duration and extent of months above freezing; second, CPDD closely aligns with the phenology of brGDGT-producing organisms, reflecting their ecological and metabolic activity. Furthermore, the Tibetan Plateau shows an overall decreasing trend in summer temperatures and an increasing trend in non-summer temperatures throughout the Holocene (Supplementary Figs. 8, 9, and 13), reflecting the pronounced seasonal temperature differences during the EMH. The rising trend in winter temperatures is also corroborated by temperature reconstructions using multiple proxies (Supplementary Fig. 12C–F), including mollusks<sup>40</sup>, *Pediastrum* algae<sup>41</sup>, and stable isotopes<sup>42,43</sup> from various regions.

### Correlation between seasonal temperature difference and organic carbon burial

We observed peak values of total n-alkane content during the EMH, exhibiting a trend consistent with TOC<sup>44</sup> (Fig. 3a, b). There is a significant positive correlation between the two, with Spearman *r* values of 0.74 ( $p < 0.01$ ) (Supplementary Fig. 14). This indicates that n-alkanes can serve as indicators of organic matter burial. Furthermore, almost all carbon chain lengths exhibited peaks during the EMH period (Supplementary Fig. 15), suggesting that both aquatic and surrounding terrestrial ecosystems had higher productivity, leading to a higher

organic carbon entering the lake sediments and being buried. It is noted that the high biological productivity and enhanced OCB in sediments during the EMH correlate well with reduced CPDD and enhanced seasonal temperature differences (Fig. 3a–c). The CPDD exhibits significant negative correlations with total n-alkane content and TOC, with Spearman's rank correlation coefficients of -0.70 and -0.54, respectively ( $p < 0.01$ , Supplementary Fig. 14). In contrast, seasonal temperature differences derived from TraCE-21ka show significant positive correlations with total n-alkane content and TOC, with Spearman's rank correlation coefficients of 0.72 and 0.54, respectively ( $p < 0.01$ , Supplementary Fig. 14). Extending back to 21 ka ago, the OCB sequence generally varies coincidentally with seasonal temperature differences changes, both exhibiting peaks between 15 ka and 6 ka and lower values before and after (Supplementary Fig. 16). We compiled TOC sequences from 25 lakes across the Tibetan Plateau (Supplementary Table 2), and found that 19 of the records exhibited peaks during the EMH period (Fig. 3d, Supplementary Figs. 17A and 18), suggesting a widespread increase in OCB in lake sediments across much of the region. Additionally, analysis of 20 pollen concentration sequences (Supplementary Table 3), which indicate plant productivity, revealed that 14 of them also exhibited peaks during the EMH (Fig. 3e, Supplementary Figs. 17B and 19), suggesting that a significant portion of the Tibetan Plateau experienced elevated vegetation productivity during this time. We thus propose that the enhanced seasonal temperature differences during this time served as a potential driving factor for OC accumulation in lake ecosystems. The reason could be that higher summer temperatures favored vegetation growth, thereby enhancing OC inputs, while lower temperatures during the non-summer months inhibited mineralization, promoting the burial of OC in lakes. The combination of abundant OC inputs and reduced mineralization facilitated significant OCB during the EMH period.

To validate this hypothesis, we conducted a simulation using the ORCHIDEE model to examine OC cycles on the Tibetan Plateau (27–35°N, 77–107°E) during the Holocene (Methods section). ORCHIDEE is a process-based dynamic vegetation model that integrates a suite of ecosystem processes, including photosynthesis, phenology, carbon allocation, carbon flow from biomass to litter, from litter to soil carbon, and heterotrophic respiration<sup>23</sup>. It is particularly well-suited for simulating land carbon dynamics across different spatial scales and assessing its potential input to lake sediments<sup>45</sup>. In this study, we used ORCHIDEE under the assumption of 100% wetland coverage, because wetlands provide a relatively simple carbon source, allowing us to focus on isolating the impacts of climate variables. Furthermore, lakes and wetlands are interconnected within regional ecosystems and hydrological cycles, making ORCHIDEE simulations valuable for understanding the influence of temperature on OCB. Our simulations, including both equilibrium and transient runs, revealed higher OC stock during the EMH compared to the Mid-to-Late Holocene (Fig. 3g, h). This suggests that the climate conditions during the EMH was more favorable for OCB. The OCB is largely determined by the balance between net primary productivity (NPP) and heterotrophic respiration (HR)<sup>11</sup>. To further explore how temperature and precipitation influence NPP and HR on the Tibetan Plateau, we compared their seasonal variability with temperature and precipitation. The results show that NPP is poorly synchronized with precipitation, particularly in lower-latitude regions (Supplementary Fig. 20). Instead, NPP increases significantly when temperatures exceed 5 °C, with the onset of growth occurring earlier in lower-latitude regions (Supplementary Figs. 20 and 21). This suggests that plant growth on the Tibetan Plateau is primarily constrained by temperature thresholds. In contrast, HR exhibits a strong seasonal correlation with temperature but is less dependent on precipitation (Supplementary Figs. 21 and 22). Additionally, the annual variations in NPP and HR throughout the Holocene demonstrate a stronger correlation with temperature than with precipitation (Supplementary Fig. 23). These findings indicate that

temperature is the dominant factor regulating both NPP and HR on the Tibetan Plateau, ultimately driving OCB dynamics.

On one hand, higher summer temperatures during the EMH favored vegetation growth, leading to relatively higher NPP (Fig. 3i, j). Although elevated temperatures may also enhance HR (Fig. 3k), the significantly higher NPP compared to HR likely resulted in more OC deposition into the sediments ( $NPP - HR = 2.04 \text{ gC/m}^2/\text{day}$ , Fig. 4a, Supplementary Fig. 24). On the other hand, the lower temperatures during the winter of the EMH reduced the decomposition rate of OC (Figs. 3i, k, 4b), allowing for substantial OC preservation (Fig. 4). Since the mid-Holocene, summer temperatures have exhibited a declining trend, corresponding to significant decreases in NPP and HR, from 5.6 to 4.8  $\text{gC/m}^2/\text{day}$  and 3.56 to 3.37  $\text{gC/m}^2/\text{day}$ , respectively (Figs. 3i–k, 4a, c, and Supplementary Table 4). Concurrently, the value of  $NPP - HR$  shows a significant decreasing trend (Fig. 3l), indicating a reduction in OC inputs. In contrast, the substantial increase in winter temperatures has extended the growing season and stimulated microbial activity (Fig. 4d), leading to a significant reduction in OCB from the mid to late Holocene (Fig. 4). Therefore, we conclude that seasonal temperature differences are the key influencing factor for OCB in lake sediments on the Tibetan Plateau. The greater temperature difference between summer and winter enhances conditions that favor OCB.

### Weakening temperature seasonality depressed organic carbon burials in lakes

We observed a decline of TOC content in the lake sediments of the Tibetan Plateau, coinciding with an upward shift in both CPDD and atmospheric  $\text{CO}_2$  concentrations around 7–6 ka BP (Fig. 3c, d, f). This phenomenon may result from a positive feedback loop between decomposition of OC,  $\text{CO}_2$  emissions to atmosphere, and climate warming (Fig. 4). Once OC is buried in sediments, it no longer participates in the short-term carbon cycle of the biosphere-atmosphere, thereby preventing greenhouse gas production in these natural systems<sup>46</sup>. During the EMH, the high OCB in lake sediments on the Tibetan Plateau somewhat suppressed the concentration of greenhouse gases in the atmosphere. However, as temperatures during the winter significantly increased, the rate of OC decomposition accelerated markedly. Coupled with the high OC content in the sediments, this led to a substantial release of  $\text{CO}_2$  into the atmosphere, further amplifying warming and accelerating OC decomposition in the sediments. As seasonal temperature differences weakened throughout the Holocene, the OCB decreased from approximately 0.4  $\text{gC/m}^2/\text{day}$  in the EMH to about 0.2  $\text{gC/m}^2/\text{day}$  in the Mid- to Late Holocene. The simulated seasonal temperature differences throughout the Holocene appears higher on the Tibetan Plateau compared to surrounding regions (Supplementary Fig. 25), but it has not been evident in the last few decades (Supplementary Fig. 26). This situation can be attributed to the region's higher winter warming rate compared to summer warming rate (Fig. 1e). Consequently, as seasonal temperature differences continue to diminish in the future, the rate of OCB in sediments may be significantly reduced. Additionally, the positive feedback mechanism, as proposed in Fig. 4, could potentially accelerate this trend.

## Methods

### Materials and chronology

A 3.44 m sediment core was retrieved from Lake Nanglalu (29.25°N, 87.23°E, 4475 m a.s.l.) in Ang Ren County, Xi Zang Autonomous Region, China, in June 2021 (Supplementary Discussion for a characterization of regional setting and sampling). The sediment core consists of alternating black, high-organic-matter sediments and gray-white clastic sediments (Supplementary Fig. 1B). We collected eight samples for accelerator mass spectrometry (AMS) radiocarbon dating (Supplementary Table 5). The AMS  $^{14}\text{C}$  samples were processed and

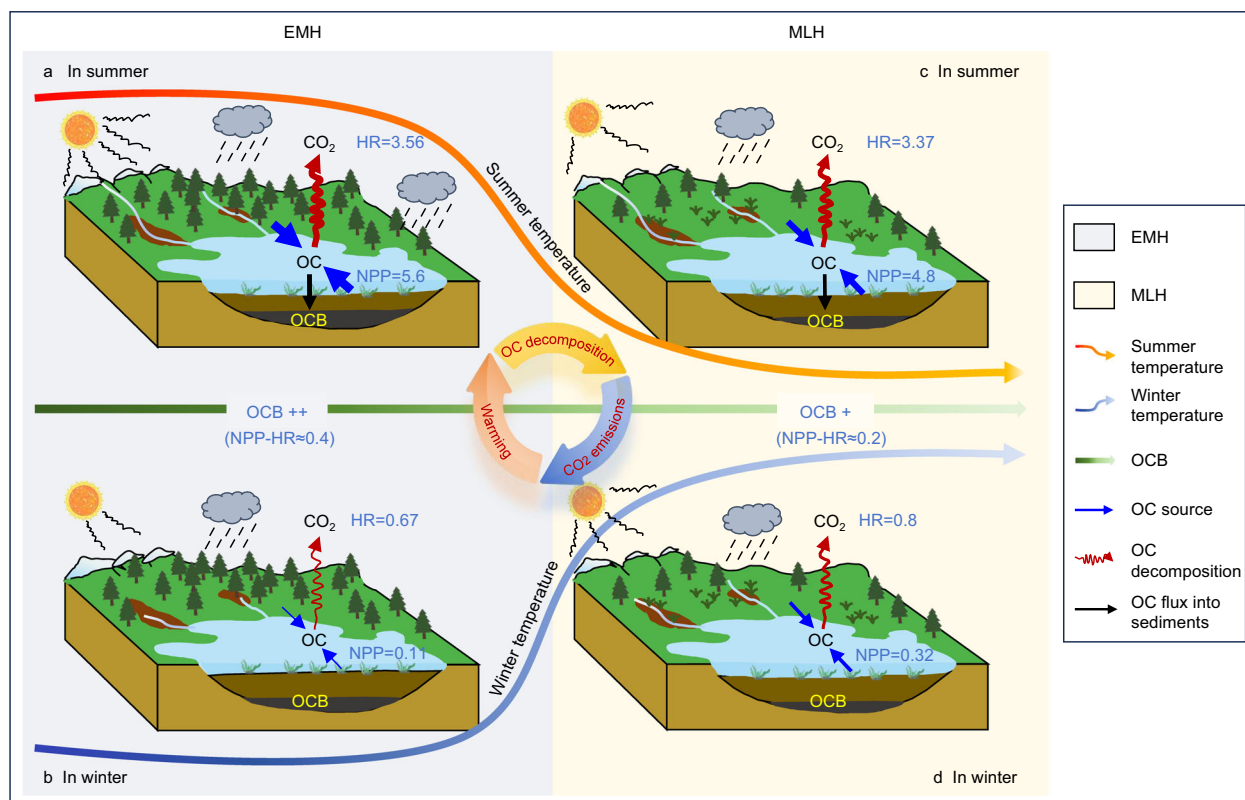


**Fig. 4 | Relationship between temperature seasonality and organic carbon burial during the Holocene.** **a** During the Early to Mid-Holocene (EMH), elevated summer temperatures enhanced both net primary productivity (NPP) and heterotrophic respiration (HR), with NPP consistently exceeding HR and resulting in an increased flux of organic carbon (OC) into sediments. **b** Lower winter temperatures during the EMH suppressed HR, favoring the preservation of OC in sediments. **c** In the Mid-to Late Holocene (MLH), decreased summer temperatures reduced both NPP and HR compared to the EMH, resulting in a diminished flux of OC into sediments. **d** Rising winter temperatures during the MLH intensified HR,

leading to greater decomposition of OC stored in sediments. The cyclic diagram illustrates the positive feedback mechanism among OC decomposition, CO<sub>2</sub> emissions to the atmosphere, and climate warming. OCB=organic carbon burial. NPP, HR and NPP-HR are expressed in gC/m<sup>2</sup>/day. The plus sign (+) represents the amount of OC entering sediments, with more plus signs indicating a higher amount. The thickness of the arrows corresponds to the intensity of each process, with thicker arrows indicating greater intensity. Detailed data comparisons are provided in Supplementary Table 4.

measured by Beta Analytic Testing Laboratory (Miami, Florida, USA). All radiocarbon dates were calibrated to calendar years BP using the IntCal20 calibration dataset<sup>47</sup>, which spans approximately from 12 ka to the present. Plant remains were used for dating all layers except those at depths of 48 cm, 70 cm, and 90 cm, where no plant remains were available, and bulk sediments were used instead. All the ages were consistent with the stratigraphic sequence, and the age-depth model was constructed using rBacon 2.2<sup>48</sup>. Our chronological framework generally aligns well with the Nanglalu record, which was dated using charcoal by Miehe<sup>44</sup> (Supplementary Fig. 1D). Previous studies indicated that the radiocarbon age of lacustrine sediments in Tibetan Plateau was significantly affected by reservoir effect<sup>49–51</sup>. However, ages from both our dataset and Miehe<sup>44</sup> suggest very young ages at the surface, and the radiocarbon results from bulk sediments at 70 cm and 176 cm are nearly consistent with the results from the charcoal at 66 cm and 170 cm, indicating that the obtained <sup>14</sup>C dates in this study are minimally impacted by the <sup>14</sup>C reservoir effect. Furthermore, the relatively shallow water levels during the Holocene and the limited input of surrounding materials further support the minimal impact of the reservoir effect.

#### Biomarker measurements

The total of 172 samples were freeze-dried and ground prior to chemical pretreatment. Approximately 0.3–10 g of each sample was ultrasonically extracted four times using dichloromethane: methanol (9:1, v/v) solution for 15 min. The total lipids were concentrated with N<sub>2</sub>

gas and saponified for over 12 h with a 6% KOH solution in methanol. Neutral lipids, including n-alkanes and brGDGTs, were further extracted through silica gel column chromatography using n-Hexane and MeOH, respectively. The n-alkanes were analyzed using an Agilent 7890B Gas Chromatograph (GC) equipped with a Flame Ionization Detector (FID). The GC system was configured with a DB-1ms capillary column (60 m × 0.32 mm × 0.25 μm), nitrogen as the carrier gas, an injection port temperature of 310 °C, and a column flow rate of 1.3 ml/min. A 1 μl sample was injected. The temperature program started at 40 °C, held for 1 min, then increased at a rate of 10 °C/min to 150 °C, and at 6 °C/min to 310 °C, with a final hold for 20 min. The BrGDGTs were analyzed using the improved chromatographic procedure of Hopmans<sup>52</sup>, with full separation of 5- and 6-methyl isomers by UPLC-APCI-MS (the ACQUITY I-Class plus/Xevo TQ-S system), equipped with two coupled UPLC silica columns (BEH HILIC columns, 3.0 × 150 mm, 1.7 μm; Waters) in series, fitted with a pre-column and maintained at 30 °C. The samples were dissolved in 1000 μl of n-hexane and 4 μl were injected. BrGDGTs were eluted at a constant flow rate of 0.4 ml/min over a period of 80 min. The mobile phases, A and B, where A = hexane and B = hexane: isopropanol (9:1, v/v), were run isocratically at 82% A and 18% B for the first 25 min, followed by a linear gradient to 65% A and 35% B from 25 to 50 min, and then to 100% B from 50 to 60 min, with an additional 20 min for re-equilibration. BrGDGTs were ionized in the APCI source at a probe temperature of 550 °C, with a corona voltage of 5.0 μV, a cone voltage of 110 V, a desolvation gas flow of 1000 l/h, a cone gas flow of 150 l/h, and a collision gas flow of

0.15 ml/min. The detection of BrGDGT isomers was performed using selective ion monitoring (SIM) mode via  $[M+H]^+$  ions at  $m/z$  744 for the C<sub>46</sub> standard and at  $m/z$  1050, 1048, 1046, 1036, 1034, 1032, 1022, 1020, and 1018 for brGDGT compounds<sup>52</sup>. The pretreatment and measurement of n-alkanes and brGDGTs were carried out at the Nanjing Institute of Geography and Limnology, Chinese Academy of Sciences.

### N-alkanes calculation

The n-alkanes were quantified using an external standard method. Five standard samples with known concentrations were tested to establish a standard curve, yielding a linear regression equation of  $y = 13.306x + 0.23$ , with an  $R^2$  value of 0.9992. In this equation,  $y$  represents the peak area of n-alkanes, which can be used to determine the relative concentration of each sample. The absolute concentration of each sample was calculated by multiplying the relative concentration by the fixed volume (400  $\mu$ l) and dividing by the weight of the sample.

### BrGDGTs-temperature calibration

The autochthonous sources of brGDGTs were first confirmed (Supplementary Discussion for a characterization of BrGDGTs-based temperature reconstruction in the Nanglalu). We further used calibration formula for regional/global lake sediments to calculate paleotemperatures (Supplementary Table 6). By comparing results from different calibration formula<sup>26–28,30,38,53,54</sup>, we found that, apart from the calibration by Günther<sup>53</sup>, which showed a reverse pattern, all other formulas yielded consistent trends in temperature variations during the Holocene. In this study, the calibration formula by Günther<sup>53</sup> were not adopted (Supplementary Table 6). We used the calibration formula from Martínez-Sosa<sup>27</sup> for further analysis, which incorporates sediment samples from 272 lakes worldwide and closely aligns with the brGDGTs distribution in Nanglalu. This formula, based on a Bayesian calibration model, accounts for temperatures during months above freezing in high-latitude or high-altitude regions. The calculated temperatures were further validated using calibration formulas from Raberg<sup>28</sup> and Wang<sup>29</sup>. All calculations were performed using Microsoft Office 2016.

### Cumulative positive degree days calculation

We analyzed 14 brGDGTs records from the Tibetan Plateau, all of which contain at least five age control points during the Holocene and have been calibrated with radiocarbon dating (Supplementary Table 1). The published brGDGTs data extraction was carried out using GetData2.2. The brGDGTs in these lakes are primarily autochthonous, and the reconstructed temperatures mainly represent lake water temperatures. Due to the presence of freezing periods in high-altitude lakes, the activity of brGDGT-producing organisms is significantly reduced during these times<sup>37</sup>. Additionally, ice layers insulate the lake water from atmospheric temperatures<sup>38</sup>, leading brGDGTs to primarily record temperature variations during the months above freezing. Here, we used monthly surface atmospheric temperatures simulated by TraCE-21ka to calculate temperature variations during months above freezing (Data source: <https://www.earthsystemgrid.org/project/trace.html>). The processing and calculations of the TraCE-21ka data were carried out in PyCharm 2021. Our analysis revealed that the duration of the months above freezing varied throughout the Holocene (Fig. 2h–l). To compare this with brGDGTs records, we calculated the mean temperature between the two 0 °C isolines. However, we found that when using mean temperatures, the reconstructed temperature curve was jagged despite, showing an inconsistent trend with brGDGTs (Supplementary Fig. 27). These discrepancies likely stem from variations in monthly temperature weights and significant expansions of duration of months above freezing in lower-latitude regions. To address this issue, we considered using cumulative positive degree days (CPDD) instead of mean temperatures, as the brGDGTs-based temperature reconstructions for most of the lakes showed a

significant Pearson correlation with CPDD (Supplementary Discussion for a characterization of BrGDGTs-based temperature reconstructions across the Tibetan Plateau). The Pearson correlation analysis was performed using IBM SPSS Statistics 25 and R4.3.3.

### TOC and pollen concentration synthesis analysis

The published TOC records from 25 sites and pollen concentration records from 20 sites on the Tibetan Plateau were collected using GetData2.2 (Supplementary Tables 2 and 3). These records span the entire Holocene and have five or more ages, all of which have been calibrated. The Bacon model was used to re-fit the age-depth relationships for all records. Furthermore, Z-score standardization was applied to these records, followed by the use of a GAM (Generalized Additive Model) to fit the results of Z-score. To investigate the representativeness of the integrated records, a statistical analysis on each individual TOC and pollen concentration record was conducted. The GAM fitting and statistical analysis were both conducted using PyCharm 2021. Among the 25 TOC records, 19 exhibited peaks during the EMH (Supplementary Fig. 18). Similarly, 14 out of the 20 pollen concentration records showed peaks during the EMH (Supplementary Fig. 19). Pollen concentration represents the number of pollen grains per unit volume or weight of a sample. We used pollen concentration as an indicator of vegetation productivity, acknowledging that variations in sedimentation rates and local wind patterns among lakes could influence pollen deposition. However, most lakes show pollen concentration peaks during the EMH, suggesting increased vegetation productivity during this period.

### Wetland carbon cycle modeling

The ORCHIDEE-PEAT land surface model was used to simulate the wetland carbon cycle processes which include vegetation photosynthesis, phenology, carbon allocation to plant biomass compartments, carbon flow from living biomass to litter pools and soil carbon pools, and heterotrophic respiration<sup>45</sup>. The simulations covered the regional range of 25–35°N and 77–107°E, at the four time points: 12 ka BP, 9 ka BP, 6 ka BP, and 3 ka BP. The simulations require meteorological forcing data, land-cover maps, and atmospheric CO<sub>2</sub> concentration data. For meteorological forcing, we bias-corrected temperature and precipitation data of TraCE based on 1901–1910 modern observational data (<https://blogs.exeter.ac.uk/trendy/protocol/>) to improve temporal and spatial resolution as well as reliability<sup>55</sup>. For each simulation, to highlight the impact of climate change on organic carbon production, we assume that all grid points in the study area are covered by 100% wetland and the atmospheric CO<sub>2</sub> concentration was fixed at 270 parts per million. We performed both equilibrium and transient simulations to model OC burial in the wetlands of the Tibetan Plateau. Four equilibrium simulations were conducted, with the model forced by the climate of 12 ka BP, 9 ka BP, 6 ka BP, and 3 ka BP, respectively. For each equilibrium simulation, the model was run for 30,000 years, by which time a steady state was reached for soil carbon pools. The transient simulation began at 12 ka, with the model run for 3000 years using the climate of 12 ka BP. This was followed by a 3,000-year simulation using the climate of 9 ka BP, a 3,000-year simulation using the climate of 6 ka BP and a 3,000-year simulation using the climate of 3 ka BP. We primarily analyzed simulated variables of net primary productivity (NPP), the decomposition of organic carbon via heterotrophic respiration (HR) and thus its potential preservation in sediments indicated by total soil organic carbon (OC). The processing and calculations of the OC simulation results were conducted in PyCharm 2021.

### ERA5 data calculation

The 2-m temperature data from 1950 to 2022 from the ERA5-Land monthly averaged dataset were used in this study<sup>15</sup>. The warming rate of the Tibetan Plateau (27–40°N, 73–103°E) was calculated by performing a linear regression on the temperature data from 1950 to 2022 for each



0.1° × 0.1° grid point, with the regression coefficient representing the warming rate (Data source: <https://climate.copernicus.eu/>). We used the average temperature from 1981 to 2010 as a baseline and calculated the differences between temperatures during various periods and this baseline to derive the anomalies for global temperatures and the winter and summer temperatures of the Qinghai-Tibet Plateau. The ERA5 data processing and calculations were performed in PyCharm 2021.

### Reporting summary

Further information on research design is available in the Nature Portfolio Reporting Summary linked to this article.

### Data availability

The authors declare that the main data supporting the findings of this study are available within the article and its Supplementary Information files. Extra data are available from the corresponding author upon request.

### References

1. Messenger, M. L. et al. Estimating the volume and age of water stored in global lakes using a geo-statistical approach. *Nat. Commun.* **7**, 13603 (2016).
2. Schlesinger, W. H. Evidence from chronosequence studies for a low carbon storage potential of soils. *Nature* **348**, 232–234 (1990).
3. Dean, W. E. & Gorham, E. Magnitude and significance of carbon burial in lakes, reservoirs, and peatlands. *Geology* **26**, 535–538 (1998).
4. Cole, J. J. et al. Plumbing the global carbon cycle: integrating inland waters into the terrestrial carbon budget. *Ecosystems* **10**, 172–185 (2007).
5. Dorrepaal, E. et al. Carbon respiration from subsurface peat accelerated by climate warming in the subarctic. *Nature* **460**, 616–619 (2009).
6. Gudas, C. et al. Temperature-controlled organic carbon mineralization in lake sediments. *Nature* **466**, 478–481 (2010).
7. Cardoso, S. J. et al. Do models of organic carbon mineralization extrapolate to warmer tropical sediments? *Limnol. Oceanogr.* **59**, 48–54 (2014).
8. Marotta, H. et al. Greenhouse gas production in low-latitude lake sediments responds strongly to warming. *Nat. Clim. Change* **4**, 467–470 (2014).
9. Yvon-Durocher, G. et al. Reconciling the temperature dependence of respiration across timescales and ecosystem types. *Nature* **487**, 472–476 (2012).
10. Yvon-Durocher, G. et al. Long-term warming amplifies shifts in the carbon cycle of experimental ponds. *Nat. Clim. Change* **7**, 209–213 (2017).
11. Liu, J. et al. Anthropogenic warming reduces the carbon accumulation of Tibetan Plateau peatlands. *Quat. Sci. Rev.* **281**, 107449 (2022).
12. Qiu, J. China: the third pole. *Nature* **454**, 393–397 (2008).
13. Xu, B. et al. Black soot and the survival of Tibetan glaciers. *Proc. Natl. Acad. Sci. USA* **106**, 22114–22118 (2009).
14. Yan, Y. et al. Surface mean temperature from the observational stations and multiple reanalyses over the Tibetan Plateau. *Clim. Dyn.* **55**, 2405–2419 (2020).
15. Hersbach, H. et al. The ERA5 global reanalysis. *Q. J. R. Meteorol. Soc.* **146**, 1999–2049 (2020).
16. Zhang, G. et al. Regional differences of lake evolution across China during 1960s–2015 and its natural and anthropogenic causes. *Remote Sens. Environ.* **221**, 386–404 (2019).
17. Yan, F. et al. Lakes on the Tibetan Plateau as conduits of greenhouse gases to the atmosphere. *J. Geophys. Res. Biogeosci.* **123**, 2091–2103 (2018).
18. Zhang, Y. et al. Natural and anthropogenically driven change of organic carbon burial rate in two alpine lakes from the southeastern margin of the Tibetan Plateau. *Catena* **247**, 108490 (2024).
19. Liu, D. et al. Substantial increase of organic carbon storage in Chinese lakes. *Nat. Commun.* **15**, 8049 (2024).
20. Ran, L. et al. Substantial decrease in CO<sub>2</sub> emissions from Chinese inland waters due to global change. *Nat. Commun.* **12**, 1730 (2021).
21. Liu, Z. et al. Transient simulation of last deglaciation with a new mechanism for Bølling-Allerød warming. *Science* **325**, 310–314 (2009).
22. Liu, Z. et al. Chinese cave records and the East Asia summer monsoon. *Quat. Sci. Rev.* **83**, 115–128 (2014).
23. Krinner, G. et al. A dynamic global vegetation model for studies of the coupled atmosphere-biosphere system. *Glob. Biogeochem. Cycles* **19**, 1–44 (2005).
24. Weijers, J. W. et al. Environmental controls on bacterial tetraether membrane lipid distribution in soils. *Geochim. Cosmochim. Acta* **71**, 703–713 (2007).
25. Peterse, F. et al. Revised calibration of the MBT-CBT paleotemperature proxy based on branched tetraether membrane lipids in surface soils. *Geochim. Cosmochim. Acta* **96**, 215–229 (2012).
26. De Jonge, C. et al. Occurrence and abundance of 6-methyl branched glycerol dialkyl glycerol tetraethers in soils: Implications for palaeoclimate reconstruction. *Geochim. Cosmochim. Acta* **141**, 97–112 (2014).
27. Martínez-Sosa, P., Tierney, J. E. & Meredith, L. K. Controlled lacustrine microcosms show a brGDGT response to environmental perturbations. *Org. Geochem.* **145**, 104041 (2021).
28. Raberg, J. H. et al. Revised fractional abundances and warm-season temperatures substantially improve brGDGT calibrations in lake sediments. *Biogeosciences* **18**, 3579–3603 (2021).
29. Wang, H. et al. New calibration of terrestrial brGDGT paleothermometer deconvolves distinct temperature responses of two isomer sets. *Earth Planet. Sci. Lett.* **626**, 118497 (2024).
30. Ding, S. et al. Distribution of branched glycerol dialkyl glycerol tetraethers in surface soils of the Qinghai-Tibetan Plateau: implications of brGDGTs-based proxies in cold and dry regions. *Biogeosciences* **12**, 3141–3151 (2015).
31. Wang, H. Y. et al. Salinity-controlled isomerization of lacustrine brGDGTs impacts the associated MBT<sup>5</sup>ME terrestrial temperature index. *Geochim. Cosmochim. Acta* **305**, 33–48 (2021).
32. He, Y. et al. Temperature variation on the central Tibetan Plateau revealed by glycerol dialkyl glycerol tetraethers from the sediment record of Lake Linggo Co since the last deglaciation. *Front. Earth Sci.* **8**, 574206 (2020).
33. Li, X. et al. Holocene climatic and environmental change on the western Tibetan Plateau revealed by glycerol dialkyl glycerol tetraethers and leaf wax deuterium-to-hydrogen ratios at Aweng Co. *Quat. Res.* **87**, 455–467 (2017).
34. Sun, Z. et al. Potential winter-season bias of annual temperature variations in monsoonal Tibetan Plateau since the last deglaciation. *Quat. Sci. Rev.* **292**, 107690 (2022).
35. Zhang, C. et al. Seasonal imprint of Holocene temperature reconstruction on the Tibetan Plateau. *Earth-Sci. Rev.* **226**, 103927 (2022).
36. Feng, X. et al. Evidence for a relatively warm mid-to late Holocene on the Southeastern Tibetan Plateau. *Geophys. Res. Lett.* **49**, e2022GL098740 (2022).
37. Loomis, S. E. et al. Seasonal variability of branched glycerol dialkyl glycerol tetraethers (brGDGTs) in a temperate lake system. *Geochim. Cosmochim. Acta* **144**, 173–187 (2014).
38. Dang, X. et al. Different temperature dependence of the bacterial brGDGT isomers in 35 Chinese lake sediments compared to that in soils. *Org. Geochem.* **119**, 72–79 (2018).
39. Bereiter, B. et al. Revision of the EPICA Dome C CO<sub>2</sub> record from 800 to 600 kyr before present. *Geophys. Res. Lett.* **42**, 542–549 (2015).

40. Dong, Y. et al. The Holocene temperature conundrum answered by mollusk records from East Asia. *Nat. Commun.* **13**, 1–9 (2022).
  41. Huang, C. et al. Western Mongolian Plateau exhibits increasing Holocene temperature. *Glob. Planet. Change.* **242**, 104577 (2024).
  42. Meyer, H. et al. Long-term winter warming trend in the Siberian Arctic during the mid-to late Holocene. *Nat. Geosci.* **8**, 122–125 (2015).
  43. Baker, J. L. et al. Holocene warming in western continental Eurasia driven by glacial retreat and greenhouse forcing. *Nat. Geosci.* **10**, 430–435 (2017).
  44. Miehe, G. et al. Föhn, fire and grazing in Southern Tibet? A 20,000-year multi-proxy record in an alpine ecotonal ecosystem. *Quat. Sci. Rev.* **256**, 106817 (2021).
  45. Qiu, C. et al. Large historical carbon emissions from cultivated northern peatlands. *Sci. Adv.* **7**, eabf1332 (2021).
  46. Mendonça, R. et al. Organic carbon burial in global lakes and reservoirs. *Nat. Commun.* **8**, 1694 (2017).
  47. Reimer, P. J. et al. The IntCal20 Northern Hemisphere radiocarbon age calibration curve (0–55 cal kBP). *Radiocarbon* **62**, 725–757 (2020).
  48. Blaauw, M. & Christen, J. A. Flexible paleoclimate age depth models using an autoregressive gamma process. *Bayesian Anal.* **6**, 457–474 (2011).
  49. Morrill, C. et al. Holocene variations in the Asian monsoon inferred from the geochemistry of lake sediments in central Tibet. *Quat. Res.* **65**, 232–243 (2006).
  50. Ma, Q. et al. Late glacial and Holocene vegetation and climate variations at Lake Tangra Yumco, central Tibetan Plateau. *Glob. Planet. Change.* **174**, 16–25 (2019).
  51. Han, J. E. et al. Vegetation and climate change since the late glacial period on the southern Tibetan Plateau. *Palaeogeogr. Palaeoclimatol. Palaeoecol.* **572**, 110403 (2021).
  52. Hopmans, E. C., Schouten, S. & Damsté, J. S. S. The effect of improved chromatography on GDGT-based palaeoproxies. *Org. Geochem.* **93**, 1–6 (2016).
  53. Günther, F. et al. Distribution of bacterial and archaeal ether lipids in soils and surface sediments of Tibetan lakes: implications for GDGT-based proxies in saline high mountain lakes. *Org. Geochem.* **67**, 19–30 (2014).
  54. Wang, M. et al. Distribution of GDGTs in lake surface sediments on the Tibetan Plateau and its influencing factors. *Sci. China Earth Sci.* **59**, 961–974 (2016).
  55. Chen, W. et al. Wetlands of North Africa during the mid-Holocene were at least five times the area today. *Geophys. Res. Lett.* **48**, e2021GL094194 (2021).
- Planning Project of NIGLAS (NIGLAS2022GS01). We thank Georg Miehe for early discussions and explorations about Nanglalu, Jacqueline F.N. van Leeuwen for providing pollen data. We thank Xiaoling Huang for the help of experiment, and thank Fei Yang, Yandong Hou, Yuye Feng, Jun Gu and Yun Cai for the sampling.

### Author contributions

H.L. designed the study. S.Z. performed experiments and wrote the draft manuscript. J.C. performed the analysis with the TraCE-21ka model. W.C. and C.Q. performed the simulation with the ORCHIDEE model. H.X. performed data analyses. P.C., Ca.Z., Ch.Z., L.C., and J.Z. revised the manuscript. All authors contributed to the discussions and revisions for the manuscript.

### Competing interests

The authors declare no competing interests.

### Additional information

**Supplementary information** The online version contains supplementary material available at <https://doi.org/10.1038/s41467-025-56399-4>.

**Correspondence** and requests for materials should be addressed to Hao Long or Jun Cheng.

**Peer review information** *Nature Communications* thanks the anonymous, reviewer(s) for their contribution to the peer review of this work. A peer review file is available.

**Reprints and permissions information** is available at <http://www.nature.com/reprints>

**Publisher's note** Springer Nature remains neutral with regard to jurisdictional claims in published maps and institutional affiliations.

**Open Access** This article is licensed under a Creative Commons Attribution-NonCommercial-NoDerivatives 4.0 International License, which permits any non-commercial use, sharing, distribution and reproduction in any medium or format, as long as you give appropriate credit to the original author(s) and the source, provide a link to the Creative Commons licence, and indicate if you modified the licensed material. You do not have permission under this licence to share adapted material derived from this article or parts of it. The images or other third party material in this article are included in the article's Creative Commons licence, unless indicated otherwise in a credit line to the material. If material is not included in the article's Creative Commons licence and your intended use is not permitted by statutory regulation or exceeds the permitted use, you will need to obtain permission directly from the copyright holder. To view a copy of this licence, visit <http://creativecommons.org/licenses/by-nc-nd/4.0/>.

© The Author(s) 2025

### Acknowledgements

This research was supported by the NSFC Basic Science Centre for Tibetan Plateau Earth System (BSCTPES) project (41988101), the National Key Research and Development Program of China (2022YFF0801103), the Strategic Priority Research Program of the Chinese Academy of Sciences (XDB40010200), the Youth Innovation Promotion Association CAS (Y201959), the National Natural Science Foundation of China (42371012, 42307556, 42371167), and the Science and Technology